

continuously varied during the conduct of the test with the magnitude of the pressure change being proportional to the total strain in the sample. The determination of the pressure at which the specimen started to strain and at fracture was accomplished by means of the slide-wire displacement circuit. By plotting the output of the slide-wire circuit versus time, the onset of strain was readily detectable. Except in the very ductile materials at high pressure, such as the 0.004% C alloy, fracture was indicated by an abrupt discontinuity in the displacement-time plot due to the stored energy in the sample at the time of fracture. In the case of the 0.004% C material at high pressure, the pressure at fracture was determined by comparing the total elongation after fracture to the displacement-time plot and the corresponding pressures.

#### POST-TEST MEASUREMENTS

The total elongation and diameter at fracture were measured using an optical comparator at  $\times 20$  magnification. A minimum of 3 diameter measurements were made at different orientations and averaged. The inaccuracy in this measurement technique was estimated to be  $\pm 0.001$  in.

A second technique used for measuring both the fracture diameter and the diameter of different regions on the fracture surface was by means of an optical microscope with a micrometer eyepiece viewing along the normal to the fracture surface.

### RESULTS AND DISCUSSION

#### Effects of Pressure Upon Ductility of Fe - C Materials

##### RELATIONSHIP BETWEEN PRESSURE AND TRUE STRAIN TO FRACTURE

True strain to fracture ( $\epsilon_f$ ) vs pressure for the materials investigated is shown plotted in Fig. 3. The statistical analysis and relationships for the best fit curves shown are summarized in Table 2.

Of initial concern was the form of the curve that best fit the data. Referring to the statistical results of Table 2, it can be seen that the correlation coefficients ( $r$ ) are quite high for all data for a linear fit. However, the correlation coefficients are the highest, and the standard deviation ( $\sigma$ ) the lowest for the annealed 0.004% C and spheroidized 0.40, 0.83 and 1.1% C materials. This indicates that these materials exhibit a linear relationship between ductility and pressure of the form:

$$\epsilon_f = A + BP \quad \text{Eq 4}$$

where  $A$  and  $B$  are the constants listed in Table 2 for a linear fit. It should be noted that since  $P$  is the independent variable, for the purpose of this analysis Eq 4 is a more appropriate relationship between strain to fracture and pressure than that given by Bridgman (Eq 1). The relationship between the constants for the two equations is simply:

$$B = \frac{1}{\beta} \text{ and } A = -\frac{\alpha}{\beta}$$

To further examine the form of the best fit relationship between strain to fracture and pressure, a test was made for a polynomial fit of the form:

$$\epsilon_f = A + BP + CP^2 \quad \text{Eq 5}$$

which is also summarized in Table 2.

It can be seen in Table 2 that the standard deviation ( $\sigma$ ) is effectively unchanged from that of a linear fit for the cases of the annealed 0.004% C and spheroidized materials. The deviation of "C" from zero is quite small, and the confidence level is much less than 95% which is the lower limit for acceptable fit. It is apparent then that no improvement results by using a polynomial rather than a linear fit for these materials.

In contrast to the above materials, there is a considerable decrease in  $\sigma$ , and the deviation of "C" from zero is quite large in the cases of the annealed

TABLE 2. Statistical Analysis of Test Data

| Material,<br>% C  | Condition    | Coefficients |       |        | Correlation<br>coefficient,<br>$r$ | Standard<br>deviation,<br>$\sigma$ | Confidence<br>level,<br>% | Deviation of<br>"C" from zero,<br>$\sigma$ units |
|---|--------------|--------------|-------|--------|------------------------------------|------------------------------------|---------------------------|--|
|   |              | A            | B     | C      |                                    |                                    |                           |  |
| <i>A—linear fit (<math>\epsilon_f = A + BP</math>)</i>            |              |              |       |        |                                    |                                    |                           |  |
| 0.004   | Annealed     | 1.968        | 0.341 | ...    | 0.984                              | 0.158                              |                           |  |
| 0.40  | Annealed     | 0.726        | 0.218 | ...    | 0.990                              | 0.216                              |                           |  |
| 0.40  | Spheroidized | 1.339        | 0.263 | ...    | 0.999                              | 0.036                              |                           |  |
| 0.83  | Annealed     | -0.043       | 0.157 | ...    | 0.968                              | 0.327                              |                           |  |
| 0.83  | Spheroidized | 0.668        | 0.216 | ...    | 0.997                              | 0.107                              |                           |  |
| 1.1   | Annealed     | -0.014       | 0.045 | ...    | 0.951                              | 0.133                              |                           |  |
| 1.1   | Spheroidized | 0.470        | 0.195 | ...    | 0.995                              | 0.175                              |                           |  |
| <i>B—Polynomial fit (<math>\epsilon_f = A + BP + CP^2</math>)</i> |              |              |       |        |                                    |                                    |                           |  |
| 0.004   | Annealed     | 2.005        | 0.276 | 0.011  | ...                                | 0.160                              | 64.04                     | .916   |
| 0.40  | Annealed     | 0.867        | 0.117 | 0.006  | ...                                | 0.015                              | 100.00                    | 39.05  |
| 0.40  | Spheroidized | 1.342        | 0.258 | 0.0005 | ...                                | 0.038                              | 35.20                     | 0.467  |
| 0.83  | Annealed     | 0.194        | 0.043 | 0.006  | ...                                | 0.119                              | 100.00                    | 9.58   |
| 0.83  | Spheroidized | 0.673        | 0.212 | 0.0003 | ...                                | 0.115                              | 13.19                     | 0.166  |
| 1.1   | Annealed     | 0.083        | 0.003 | 0.002  | ...                                | 0.082                              | 99.99                     | 3.967  |
| 1.1   | Spheroidized | 0.526        | 0.162 | 0.001  | ...                                | 0.163                              | 84.4                      | 1.418  |

**ATMOSPHERIC PRESSURE MECHANICAL PROPERTIES**

The atmospheric pressure tensile properties were obtained using an Instron Tensile Machine with a 0.050 in./in. strain rate. The measured properties are summarized in Table 1. It should be noted that the actual form of the true stress-true strain relationship for the materials utilized herein was a power function. Thus the strain hardening coefficient ( $n$ ) in Table 1 is not the same as the  $N$  in Eq 2 where a linear relationship has been assumed.

**Equipment**

The pressure device utilized consisted of a Bridgman piston-cylinder type 30 kbar hydrostatic pressure system (1). The main pressure cylinder, which consisted of an autofrettaged externally tapered inner liner and matching restraining jacket, contained a  $\frac{3}{4}$ -in. diam 8-in. long pressure cavity. Both liner and jacket were fabricated of 250 grade maraging steel. Electrical leads were introduced into the pressure cavity through the bottom closure for the purpose of measuring pressure and strain of the sample.

Pressure measurement was accomplished by means of a 120-ohm manganin coil comprising one arm of a bridge which also contained a Foxboro recorder. The estimated inaccuracy in pressure measurement was  $\pm 2\%$ .

The fixture for the conduct of the tensile test under pressure, which fitted inside of the pressure cavity, consisted of four legs. Two legs were stationary and bore against the bottom closure of the pressure cavity. The remaining two legs were driven downward by the advancing main pressure piston which introduced tensile forces in the sample. The strain in the sample during testing was measured by means of a slide-wire resistance circuit which measured the relative displacement between the stationary and movable legs of the fixture. Displacement as a function of time was continuously recorded using an X-Y recorder. The circuit had an output of 55.0 mv/in. of displacement.

**Procedures****HIGH-PRESSURE TENSILE TESTING**

The high-pressure tensile tests were conducted at a constant displacement rate of 0.050 in./min.

Since the permissible displacement of the main pressure piston was fixed by the length of the tensile specimen and associated fixture, a means for varying the test pressure had to be provided. This was accomplished by pre-charging the pressure cavity to various selected levels from 0.5 to 3.0 kbars with nitrogen gas which also acted as the pressure transmitting media.

The strain in the specimen was accomplished by the advance of the main piston. Thus, the pressure

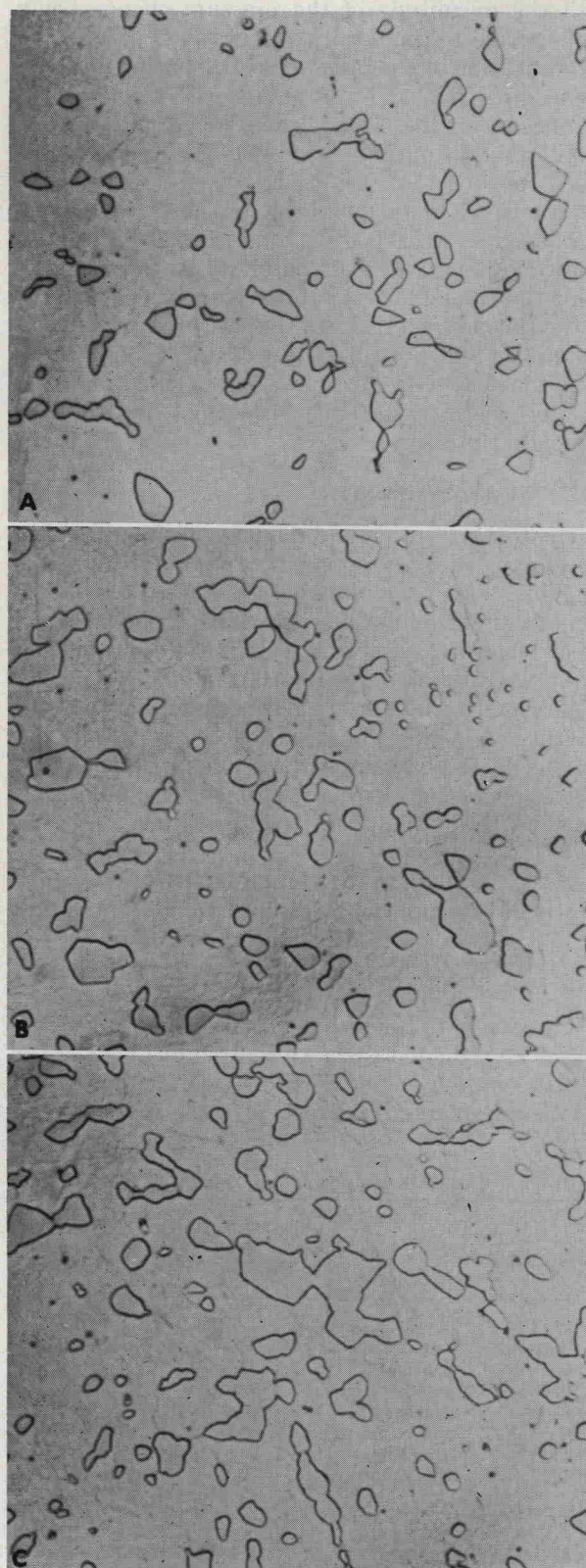


Fig. 2. Microstructure of spheroidized Fe-C materials. (A) 0.40% C; (B) 0.83% C; (C) 1.1% C.  $\times 1000$ .